Journal of Molecular Structure 1049 (2013) 78–89

Contents lists available at SciVerse ScienceDirect

Journal of Molecular Structure

journal homepage: www.elsevier.com/locate/molstruc

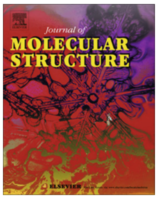

Synthesis and mesomorphic behaviour of achiral four-ring unsymmetrical bent-core liquid crystals: Nematic phases

Manoj Kumar Paul [a,*], Gayatri Kalita [a], Atiqur Rahman Laskar [a], Somen Debnath [a], Venkatesh Gude [a], Dipika Debnath Sarkar [a], Golam Mohiuddin [a], Sanjay Kumar Varshney [b], V.S. Nandiraju Rao [a,*]

[a] *Department of Chemistry, Assam University, Silchar, India*
[b] *Centre for Soft Matter Research, Bangalore, India*

HIGHLIGHTS

- Design of achiral four-ring unsymmetrical bent-core liquid crystals resembling true hockey-stick shaped compounds.
- Synthesized compounds are characterized and Phase behaviour is discussed.
- Wide range nematic phases and stable supercooling of nematic phase are observed.
- Molecular interactions viz., end chain length plays an important role thermal stability of nematic phase.

ARTICLE INFO

Article history:
Received 7 April 2013
Received in revised form 10 June 2013
Accepted 17 June 2013
Available online 24 June 2013

Keywords:
Bent-core
Azo group
Nematic phase
Liquid crystal
DFT calculation

ABSTRACT

Achiral four ring unsymmetrical bent-core liquid crystals derived from 3-amino-2-methylbenzoic acid have been designed and synthesized with an imine, ester and photochromic azo linking moieties. These hockey-stick shape resembling bent molecules possess an alkoxy chain at one end of the molecule and methyl or methoxy group at the other end. The synthesis, phase transition temperatures and characterization of phase behaviour are discussed. The molecular structure characterization is consistent with data from elemental and spectroscopic analysis. The materials thermal behaviour and phase characterization have been investigated by differential scanning calorimetry and polarizing optical microscopy. All these compounds exhibit enantiotropic nematic phase over wide temperature range. Stable supercooling of nematic phase has been observed in methoxy homologues. The density functional theory (DFT) calculations were performed to obtain the stable molecular conformation, polarizability, dipole moment, Highest occupied molecular orbital (HOMO), Lowest unoccupied molecular orbital (LUMO) energies and bending angle of the compound.

1. Introduction

Bent core liquid crystals [1–4] have become major topic of research in material science due to their interesting properties. The discovery of spontaneous polarity [5], chirality [6], giant flexo-electric response [7], 2D polarization splay modulated and layer undulated smectic phases [8–14], in achiral bent–core mesogens (BCMs) led to several questions to be addressed related to structure–property relationship. The manifestation of the nematic (N) phase in materials of BCMs is relatively scarce due to the strong tendency for smectic layering generated by the close packing of the kinked (bent) molecules promoted by the strong aromatic core–core interactions [15–17]. The derivatives of 1,3-disubstituted phenyl ring with a substituent in 2- or 4-positions of five-ring system mostly exhibited N phase [18–26]. The increase of a bent angle at the apex by the replacement of 1,3-substituted phenyl ring by a 2,5-substitued heterocycles like oxadiazole/thiadiazole [27–31], unsymmetrical hockey-stick molecules [32], or dimesogens comprised of rod-like and bent units [33–35] (with an overall reduction in bent angle) also yielded the N phases at high temperatures in addition to layered smectic or columnar phases. Hence the realization of the N phase in BCMs with suppression of layered phases is dependent on the molecular architecture with extended aromatic cores and/or relatively shorter terminal chains, lateral and/or transverse polar substituents or the increase of the bend angle promoted by rigid extended five-membered heterocycle ring at the centre.

The nematic phases exhibited by BCMs are of special importance viz., (a) biaxiality [36–39], (b) nematic phases composed of tilted smectic (SmC-type) cybotactic clusters (NcybC) with strongly tilted aromatic cores [15,39–44] (c) ferro-nematic phase which is yet to be corroborated with further experimental evidence

---

* Corresponding authors.
E-mail addresses: paulmanojaus@gmail.com (M.K. Paul), drnvsrao@gmail.com, nandirajuv@gmail.com (V.S. Nandiraju Rao).

0022-2860/$ - see front matter © 2013 Elsevier B.V. All rights reserved.
http://dx.doi.org/10.1016/j.molstruc.2013.06.044

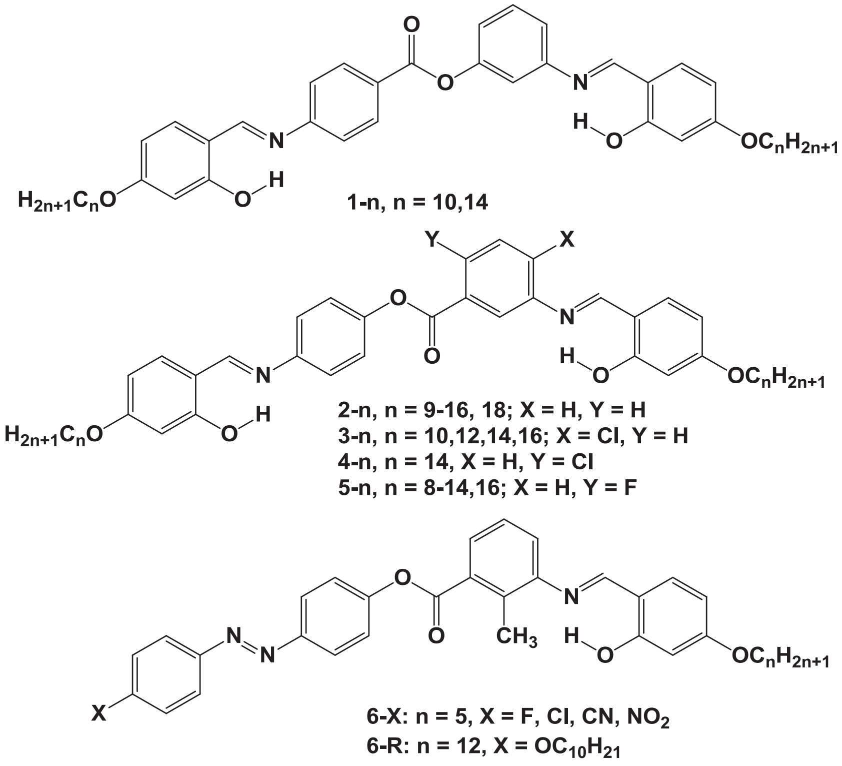

Fig. 1. Molecular structure of few four-ring unsymmetrical bent-core molecules.

(ferroelectric switching?) [40,45] (d) Negative bend-splay elastic anisotropy [46] for the generation of long thermal range blue phases etc. Even though the conclusive experimental proof of a macroscopic biaxiality in nematic phases is still eluding, the X-ray diffraction (XRD) measurements unequivocally confirmed the biaxial molecular aggregates of cybotactic nematic phases composed of SmC-like clusters in BCMs.

The realization of nematic phases in five-ring bent-core compounds as such are rare and limited [16–24,39–43]. Most of the four-ring bent-core compounds reported earlier are either mesomorphic (layered smectic phases) or non-mesomorphic [26,32,47,48]. However we reported few four-ring compounds as depicted in Fig. 1, exhibiting banana phases (**1-n**, **2-n**, **3-n**, **4-n** and **5-n**) [12–14,48] and some others possessing polar or alkyloxy moiety at one end of the molecule exhibiting nematic phase (**6-X**, **6-R**) [44,49–51]. Hence any attempt to synthesize compounds with a combination of different linking groups, and a variety of substituents is still a challenging goal for chemists that can lead to detailed understanding of structure–property relationship as well as its functional characteristics. It cannot be taken for granted a priori that all the new bent-core molecular structures would still be able to form nematic phase, and it is also conceivable that there would be a complete loss of mesophase behaviour in some cases. In the present study we discuss the synthesis of four-ring bent core hockey-stick shaped compounds and the influence of the end alkyl/alkyloxy chains in the enhancement of nematic phase range.

2. Results and discussion

The four-ring bent-core molecule possessing three linkages viz., imine linkage stabilized by H-bonding with ortho hydroxyl group, an ester linkage and photochromic azo linkage had been designed with smaller alkoxy chains at one end and methyl or methoxy moieties at the other end. The compounds that undergo a reversible photochemical reaction where an absorption band in the visible part of the electromagnetic spectrum changes dramatically in strength or wavelength are classified as photochromic compounds due to trans–cis isomerization of azo linkage. The presence of ortho hydroxyl group in benzylidene moiety enhances the stability of the imines through intramolecular H-bonding to overcome the hydrolytic instability of the molecules towards moisture and also enhances the transverse dipole-moment. The resorcylidene core is more stable towards to atmospheric hydrolysis. The liquid crystalline phases (smectic to nematic or nematic to isotropic) of these materials possessing a photochromic azo group can be induced by the *trans*-to-*cis* isomerization under the influence of UV irradiation [52]. The synthesis of the compounds as detailed in Scheme 1 was carried out following the procedure described in experimental section.

The alkylation with alkyl bromide of 2,4-dihydroxybenzaldehyde takes place preferentially with 4-hydroxyl group rather than 2-hydroxyl group [53,54]. 2-hydroxyl group is bonded through hydrogen bonding with aldehyde carbonyl oxygen which is evidenced in NMR spectra ($\delta = 11.44$) (Electronic supplementary information (ESI) Table S1). The free 4-hydroxyl ($\delta = 5.55$) moiety readily undergoes alkylation to yield 4-alkoxy 2-hydroxy benzaldehyde preferentially. Further the alkylation reaction was carried out at $T < 50$ °C such that the activation energy required to break the H-bonding and to participate in alkylation reaction is not sufficient. Use of low boiling point solvent acetone (B.P. 56 °C) instead of high boiling point solvent like cyclohexanone promoted the formation of monoalkylation rather than dialkylation. 4-alkoxy 2-hydroxy benzaldehyde was purified by column chromatography using silica gel (60–120 mesh) as stationery phase and petroleum ether or hexane or $CHCl_3$-hexane as eluent.

The 4-n-alkyloxy 2-hydroxy benzaldehyde was then condensed with 3-amino 2-methyl benzoicacid to yield the Schiff bases viz., 3-[4-n-alkyloxy2-hydroxybenzylidene] 2-methyl benzoic acids (ESI Table S3) in good yields. 3-[4-n-Butyloxy 2-hydroxy benzylidene]

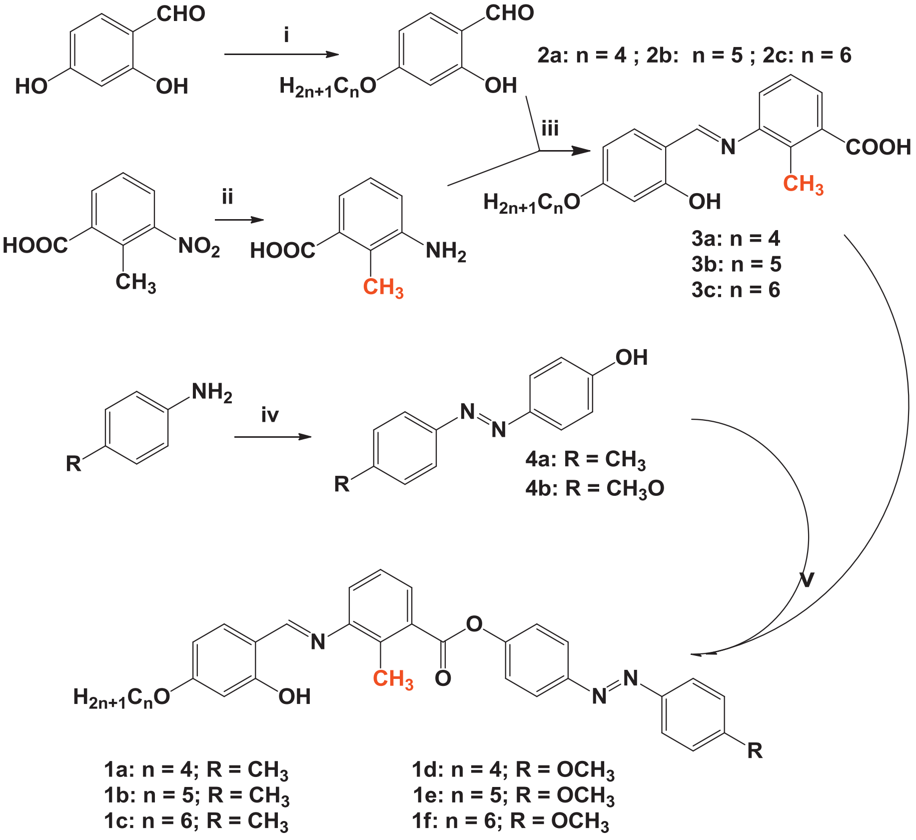

Scheme 1. Synthetic details of compounds **1a–1f**. Reagents and conditions (i) dry acetone, $KHCO_3$, $C_nH_{2n+1}Br$ (n = 4, 5, 6), KI (catalytic amount); (ii) 5% Pd/C, H_2, EtOAc, stirring 48 h; (iii) abs EtOH, AcOH, Δ, 6 h; (iv) HCl, $NaNO_2$, 0–5 °C, Phenol, NaOH; and (v) dry DCM, DMAP, DCC, stirring 48 h.

2-methyl benzoicacid was further esterified with 4-methyl azophenol or 4-methyloxy azophenol using DCC–DMAP reaction to yield the designed products **1a–1f**, following the procedure reported earlier [55]. The esterification reaction preferentially undergoes between the 4-hydroxyl group of the 4-substituted azophenol (ESI Table S2, δ = 5.56 or 5.65) rather than 2-hydroxyl group (ESI Table S3, δ = 13.49, hydrogen bonded proton) of 3-[4-n-butyloxy 2-hydroxy benzylidene] 2-methyl benzoicacid. 2-hydroxyl group in 3-[4-n-butyloxy 2-hydroxy benzylidene] 2-methyl benzoicacid is bonded through hydrogen bonding with nitrogen of imine linkage which is evidenced in NMR spectra (δ = 13.49) (ESI Table S3). Further the alkylation reaction was carried out at room temperature 25 °C such that the activation energy required for breaking the H-bonding and to participate in esterification reaction is not sufficient.

Elemental analyses of all the compounds were consistent with the proposed molecular formulae. All the compounds were characterized by FTIR, UV–Visible and ^1H NMR studies. The infrared spectra of all the compounds exhibited characteristic bands of imine (—CH=N—) stretching vibration 1604∼1612 ($\nu_{CH=N}$, imine), 1740 ± 5 ($\nu_{C=O}$, ester), 3200 ± 50 (ν_{O-H}, H-bonding). The phenolic C—O stretching vibration was observed around 1290 cm^{-1}. The ^1H and ^{13}C NMR data is consistent with chemical shift values of the protons in different chemical environment of the molecules. The analysis of the NMR data of the target molecules is furnished in ESI (Fig. S4).

3. Thermal behaviour: DSC and polarized optical microscopy

Polarized optical microscopy (POM) studies were performed to examine the liquid crystalline phases, to confirm the observed phase transition temperatures by POM with the data obtained from differential scanning calorimetry (DSC), and the influence of alkoxy and alkyl groups on the width of temperature range of the phases. The phase transition temperatures, transition enthalpies and entropies are presented in Table 1. A representative DSC thermogram of the compound **1a** is presented in Fig. 2. The DSC thermograms of other compounds **1b–1f** are presented in ESI (Figs. S2a–e). All the compounds exhibited fluid Schlieren textures in the enantiotropic mesomorphic phase regions with integer and half-integer disclinations in the entire phase range indicating a nematic phase. The representative textures of nematic phase viz., a nematic droplet texture, Schlieren like/or marble textures exhibited by the compounds **1a–f** are presented in Fig. 3. Moreover they display a wide thermal range of nematic phase. The nematic phase range ($\Delta T_N = T_{NI} - T_{KN}$) of the methoxy homologues is much larger than the methyl homologues. It reflects that the presence of oxygen atom in the terminal methoxy moiety has important influence on the mesophase thermal stability as well as phase thermal range.

The large enthalpy values recorded at the crystal to nematic (Cr–N) phase transition in the heating cycle indicate strong interactions (van der Waals type) between the end chains of neighbouring molecules. From the lower enthalpy values in the cooling cycle than in the heating cycle recorded at the crystal to nematic (Cr–N) phase transition in DSC measurements, it appears that strong interactions (van der Waal type) between end chains of neighbouring molecules keep them static in the crystalline phase before the transition to LC state in the heating cycle. However these interactions are totally disrupted in the nematic phase allowing the end chains to freely rotate. Hence, in cooling cycle, lowering of nematic to crystalline (N–Cr) transition temperature of the order of 18 ± 5 °C for methyl homologues and 45 ± 17 °C for methoxy homologues is required to reestablish the crystalline phase from

Table 1
Phase transition temperatures (°C) and nematic phase thermal range of the compounds **1a–1f** recorded for second heating (first row) and second cooling (second row) cycles at 5 °C/min from differential scanning calorimetry (DSC) and confirmed by polarised optical microscopy (POM). The enthalpies (ΔH in kJ/mol) and entropies (ΔS in J/mol/K), respectively, are presented in parentheses. $\Delta T_N = T_{NI} - T_{Cr-N}$, is in cooling cycle, where T_{NI} is nematic-isotropic transition temperature and T_{Cr-N} crystal–nematic transition temperatures respectively.

Compounds	*n*	R		$\Delta T_N = T_{NI} - T_{Cr-N}$
1a	4	Me	Cr 143.3 (37.2, 89.5) N 169.5 (0.34, 0.77) Iso Cr 125.9 (31.0, 78.0) N 164.7 (0.32, 0.74) Iso	26.2 38.8
1b	5	Me	Cr 137.2 (30.6, 74.6) N 164.3 (0.36, 0.82) Iso Cr 116.6 (27.5, 70.6) N 163.2 (0.32, 0.75) Iso	27.1 46.6
1c	6	Me	Cr 138.0 (45.2, 109.9) N 163.8 (0.46, 1.06) Iso Cr 111.6 (25.3, 65.8) N 161.9 (0.42, 0.98) Iso	25.8 50.3
1d	4	MeO	Cr 155.8 (96.5, 224.9) N 194.5 (1.37, 2.94) Iso Cr 97.0 (71.6, 193.5) N 191.8 (1.17, 2.53) Iso	46.6 99.0
1e	5	MeO	Cr 142.9 (55.7, 131.8) N 176.2 (0.49, 1.09) Iso Cr 102.1 (43.3, 120.8) N 174.2 (0.59, 1.32) Iso	43.7 77.8
1f	6	MeO	Cr 143.2(45.2, 108.7) N 189.4 (0.41, 0.89) Iso Cr 116.4 (41.8, 107.0) N 188.8 (0.42, 0.92) Iso	47.0 72.4

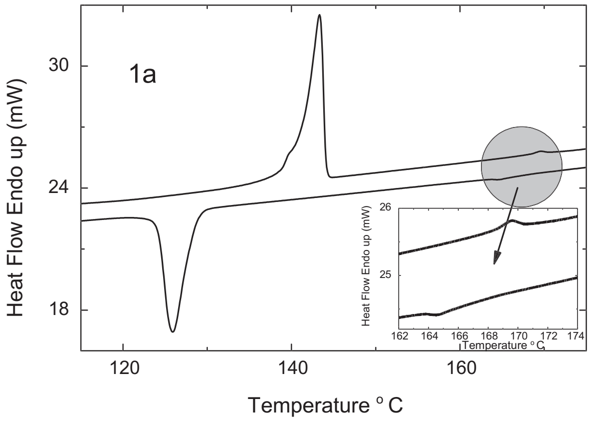

Fig. 2. Representative differential scanning calorimetry (DSC) of compound **1a** in the second heating and cooling at 5 °C/min.

LC phase and indicated the stable supercooled nematic phase. It is clearly demonstrated that in methoxy homologues the existence of stable supercooled nematic phase decreased with an increase in the alkyl chain length (for lower homologues) reflecting the restriction in free rotation of alkyl chains.

The small enthalpy changes observed at the liquid crystalline nematic phase possessing orientational order to isotropic liquid with random ordering of molecules are indicative of smaller changes in the molecular ordering. In fact the slightly higher enthalpy changes exhibited by the methoxy homologues (**1d–1f**, $\Delta H = 0.40–0.50$) than the smaller enthalpy exhibited by methyl homologues (**1a–1c**, $\Delta H = 0.28–0.35$) is indicative of stronger dipolar association of molecules. The enthalpy values at the nematic-isotropic transition temperature are in conformity with reported data for such systems [56]. A comparison of the width of the nematic phase range (ΔT_N) as a function of chain length in the cooling cycle revealed that width of nematic phase increases with increasing chain length for methyl homologues while a decreasing trend for methoxy homologues was observed (Fig. 4).

A comparison of the nematic-isotropic clearing temperature of the compounds with similar molecular structure (**6-X**) possessing polar groups like fluoro, chloro, cyano and nitro substituents instead of methyl or methoxy substituents revealed that T_{NI} increases in the order of F, Me, MeO, Cl, NO_2, CN substituents. The nematic thermal phase range (ΔT_N) also followed almost same trend. In another compound (**6-R**) possessing an identical aromatic core extended with long aliphatic chains an unusual temperature dependence of smectic layer structure associated with the nematic–smectic C phase transition and smectic-C-type diffuse layer reflection over the entire nematic temperature range are reported [44]. The smectic-C-type diffuse layer reflections are an indication of nematic phase possessing cybotactic SmC type clusters abbreviated as cybotactic nematic phases (N_{cybC}). The optical textures exhibited by **1a–1f** resemble the textures observed in nematic phase of the compound 6-**R**, the nematic phase can also be regarded as cybotactic nematic phase.

3.1. Optical absorption and emission studies

All the compounds (**1a–1f**) reported here are azobenzene derivatives which are interesting materials because of their *trans–cis* or *cis–trans* isomerisation and occurs due to external stimuli for ex. irradiation by UV light, mechanical stress, electrostatic simulation or recovering the thermodynamic stability. Before irradiating the compounds synthesised in this study, it is important to explore their light absorption characteristics. The UV–Visible absorption spectra of compounds **1a–f** ($c = 10^{-5}$ M solution in $CHCl_3$) revealed strong absorption for the methyl (**1a–c** at 340 nm) and methoxy (**1d–f** at 348 nm) homologues with a large molar extinction coefficient ($\varepsilon = 47{,}400–37{,}900\ \mathrm{L\ mol^{-1}\ cm^{-1}}$), which reflected the symmetry allowed π–π^* transition of chromophore in the molecule [57]. However a weak absorption in the visible region ~450 nm ($\varepsilon = {\sim}200\ \mathrm{L\ mol^{-1}\ cm^{-1}}$) corresponding to symmetry forbidden n–π^* transition [58,59] was also observed. The UV–Visible absorption spectra of **1a** and **1d** shown in Fig. 5 were obtained in 1×10^{-5} M solutions using $CHCl_3$ as solvent in three different conditions viz., (a) virgin sample solution, (b) solution after exposure to UV light for 2 h and (c) solution kept in dark for 12 h. From the analysis of the spectra it can be readily seen that there is change in absorption intensity and peak position of each compound from virgin sample solution to UV light irradiated solution and solution kept in dark for 12 h. The high and low intense absorption bands centred at 336 nm and 445 nm are due to the π–π^* and n–π^* electronic transitions, respectively [60–62]. The freshly prepared dilute solution of the azo compounds when irradiated with UV light for 2 h, the resulting UV–Visible spectra illustrated that the π–π^* transition band is blue shifted (~8–10 nm) with an decrease in intensity of the band for methoxy compounds (**1d–1f)** whereas the shift of π–π^* band for methyl compounds (**1a–1c**) is negligible. However, the opposite phenomenon occurred in the case of n–π^* band. The intensity of the n–π^* band of the freshly prepared solution is less than for the UV irradiated solution. When the solution was kept

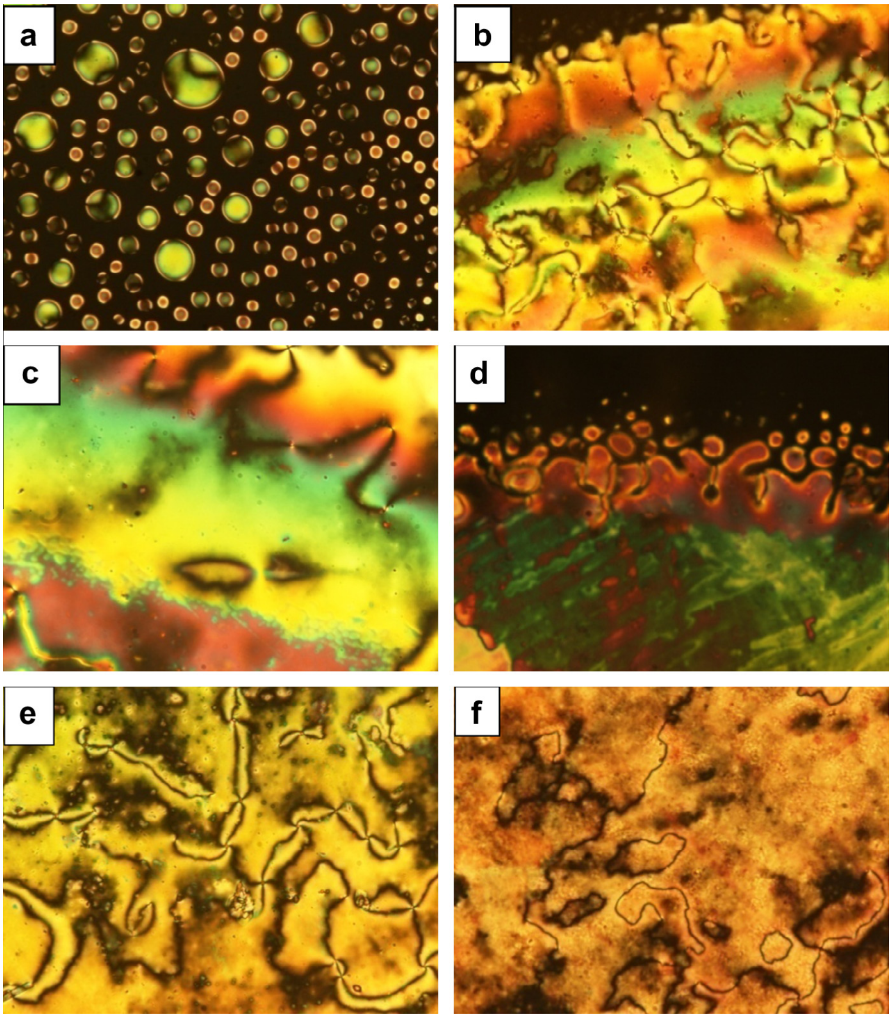

Fig. 3. Microphotograph of compounds **1a–f** in nematic phase in cooling cycle. (a) Nematic droplet texture of **1a** at 159.8 °C. (b) Schlieren texture of **1b** at 162.0 °C. (c) Schlieren texture of **1c** 161.4 °C. (d) Nematic droplets texture of **1d** at 191.6 °C. (e) Schlieren texture of **1e** at 170.3 °C. (f) Marble texture of nematic phase exhibited by **1f** at 186.5 °C.

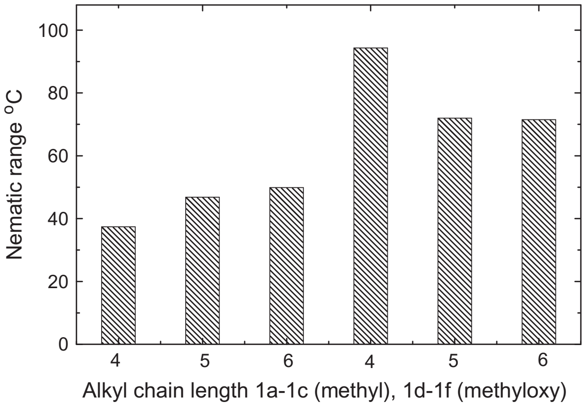

Fig. 4. Variation of nematic phase range as function of increasing chain length for methyl **1a–1c** and methoxy **1d–1f** homologues in the cooling cycle.

in dark for 12 h the peak position of the high intense π–π* band and intensity of n–π* band were gradually shifted and the UV–Visible spectra appeared closer to the UV spectra of virgin solution (ESI: Fig. S3a–d).

As expected, the symmetry allowed high intense π–π* absorption band decreased progressively while the symmetry forbidden low intense n–π* absorption band increased after UV irradiation due to the *trans–cis* photo-induced isomerisation. If we consider only the azobenzene moiety the symmetry for *trans* [E-isomer] azobenzene is C_{2h} and for *cis* [Z-isomer] azobenzene is C_2 and hence the symmetry is breaking down from *trans* to *cis* isomer indicating a less conjugation as shown in Fig. 6. Thus it is obvious that after UV irradiation there should be shift of π–π* band towards the lower wavelength. As the symmetry is transformed from *trans* to *cis* isomer, an increase in the intensity of n–π* band was observed. Actually the n–π* transition occurs from the non bonding (*n*) electrons of nitrogen atom shift to the π* orbital of the molecule. Further the difference in hypsochromic effect of the compounds **1a–1c** and **1d–1f** after UV light irradiation might be simply associated with the difference in the end methyl or methoxy substituents at the azo end. Further investigation to sort out the exact reason for this anomaly between methoxy and methyl compounds is in progress. Therefore the change in absorbance with respect to the time exposed to UV-light irradiation is only because of *trans–cis* isomerization and not due to aggregate formation. To examine the aggregates formation (i) a study on varying the concentration of each compound in $CHCl_3$ and (ii) in other solvents to evaluate the influence of polarity of solvents (Tetrahydrofuran, Toluene, Dimethylformamide) was carried out and it revealed the absorption at two wavelengths (ESI Fig. S4). Secondly the change

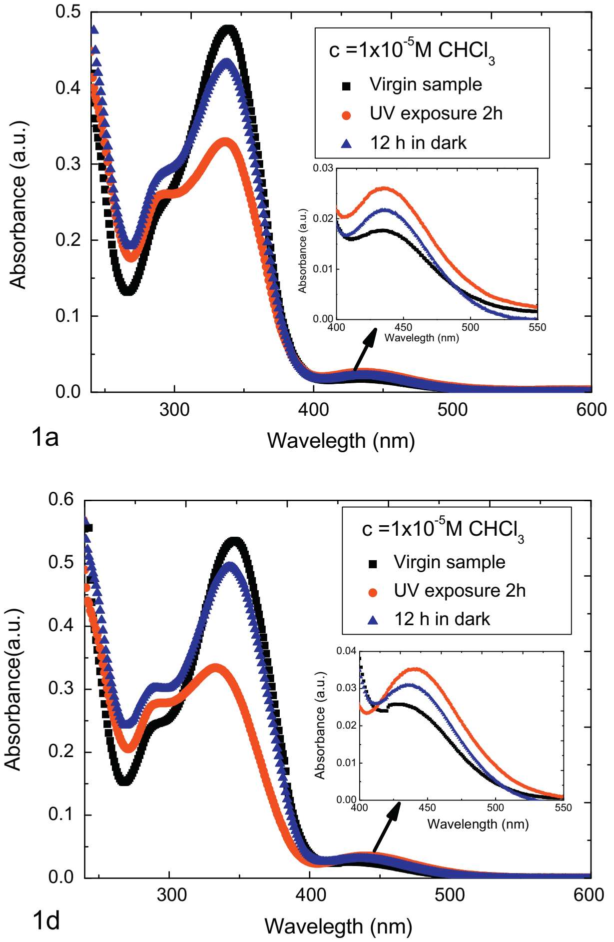

Fig. 5. UV–Visible absorption spectra of **1a** (methyl homologue) and **1d** (methoxy homologue) in chloroform ($c = 1 \times 10^{-5}$ M) and changes in the absorption spectrum with respect to exposure time to UV light and in absence of light.

of absorbance with respect to the time exposed to UV light and in dark revealed the *cis–trans* isomerism which is in conformity of earlier reports in azo based compounds exhibiting liquid crystalline behaviour. All the compounds upon illumination with UV light, a decrease in N–I transition temperature was observed in POM by 1–5 K depending on the time of exposure.

4. DFT studies

Density functional theory (DFT) investigations have been performed on all the compounds **1a–1f** to obtain more insight related to the molecular conformation, molecular polarizability, dipole moment, HOMO, LUMO energies and bending angle. Full geometry optimization had been achieved without imposing any constraint using Gaussian 09 program package [63]. Spin-restricted DFT calculations were carried out in the framework of the generalized gradient approximation (GGA) using Becke3-Lee–Yang–Parr hybrid functional (B3LYP) exchange–correlation functional and the 6-311G(d,p) basis set [64,65]. B3LYP functional with the standard basis set 6-311G(d,p) have been used due to its successful application for larger organic molecules as well as hydrogen bonded systems [66–70]. The molecular dipole moment plays an important role in the determination of electrostatic intermolecular interactions [71]. Polarizabilities play a key role to understand molecular optical properties. The results are summarized in Tables 2 and 3. For all the molecules (**1a–1f**) the polarizability $\boldsymbol{\alpha}$ is largest along the molecular long *X*-axis (see Table 3).

According to theoretical predictions, phase behaviour of liquid crystalline compounds is closely related to the bending angle of the compound [70]. DFT study revealed a bending angle of 143–146° (see Fig. 7) for all the compounds. As the bending angle increases, the bent core compounds are rather prone to exhibit nematic phase rather than smectic phases. However due to the many possible conformations the calculated bending angle may not exactly reflect the realistic conformation for each compound in a liquid–crystalline phase but gives an approximate estimation. Hence the asymmetry parameter (η) which is dependent on bending angle [65], as a possible indication is given by $\eta = [(\alpha_{YY} - \alpha_{ZZ})/(\alpha_{XX} - \alpha^{iso})]$, where $\alpha_{XX,}$ $\alpha_{YY,}$ and α_{ZZ} are the principle components of the molecular polarizability tensor and α^{iso} is the isotropic molecular polarizability with $\alpha^{iso} = (\alpha_{XX} + \alpha_{YY} + \alpha_{ZZ})/3$). Due to the large bending angle, the asymmetry parameter η is found to be very small. The asymmetry parameter, η, which defines the polarizability characteristics of the molecules, is rather very small reflecting the importance of its contribution to the mesomorphism. The asymmetry parameter is found to be lower than the values reported earlier [50,51]. The large bending angle ~146° in these compounds also contributes in the formation of nematic phases. The principle components of polarizability tensor α_{YY}, and α_{ZZ} are rather small in comparison to polarizability in longitudinal direction of the molecule (α_{XX}). Polarizability tensor along the molecular long axis i.e. α_{XX} is larger for **1d–f** (due to the presence of oxygen

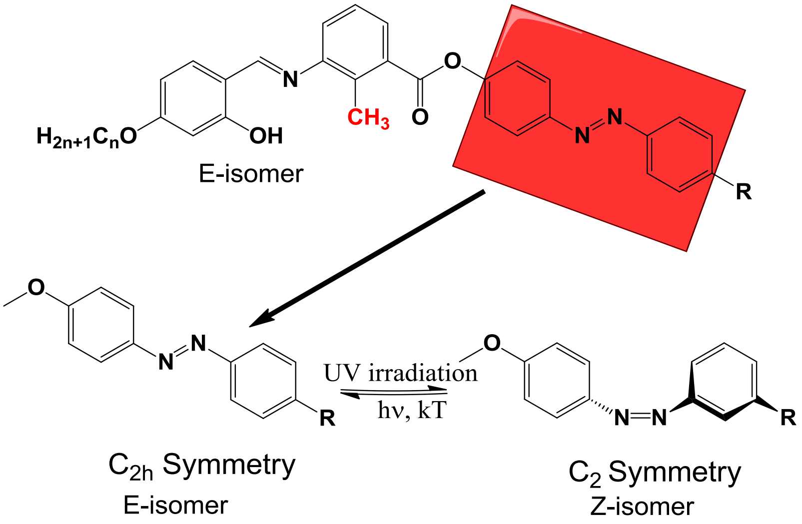

Fig. 6. Molecular structure of *trans* (E) and *cis* (Z)-isomers of compound.

Table 2
DFT calculated dipole moment components (μ_X, μ_Y, μ_Z), and the resultant dipole moment (μ), bending angle and molecular length of the compound.

Compounds	Dipole moment (Debye)				Bend angle (degree)	Molecular length (Å)
	μ_x	μ_y	μ_z	$\mu_{resultant} = (\mu_X^2+\mu_Y^2+\mu_Z^2)^{1/2}$		
1a	2.72	1.74	3.27	4.60	142	29.7
1b	2.89	2.31	2.60	4.52	143	31.1
1c	2.76	1.62	3.33	4.62	142	32.1
1d	1.57	3.25	1.18	3.80	146	31.2
1e	1.60	3.13	1.19	3.72	146	32.4
1f	1.59	3.15	1.24	3.74	146	33.7

Table 3
DFT calculated principal polarizability components (α_{XX}, α_{YY}, α_{ZZ}), isotropic polarizability $\alpha^{iso} = (\alpha_{XX} + \alpha_{YY} + \alpha_{ZZ})/3$, polarizability anisotropy $\Delta\alpha = [\alpha_{XX} - (\alpha_{YY} + \alpha_{ZZ})/2]$, and asymmetry parameter, $\eta = [(\alpha_{YY} - \alpha_{ZZ})/(\alpha_{XX} - \alpha^{iso})]$. Parameters relative to the molecular polarizability tensor in the Cartesian Reference frame.

Compounds	α_{XX}	α_{YY}	α_{ZZ}	α_{iso}	$\Delta\alpha$	η_α
1a	885	337	265	496	584	0.18
1b	913	342	276	510	604	0.16
1c	919	359	286	521	597	0.18
1d	946	315	269	510	654	0.10
1e	965	323	280	523	664	0.10
1f	981	334	291	535	669	0.09

All polarizability components and the anisotropy parameter are calculated in Bohr^3 (with 1 Bohr = 0.52917 Å).

atom of methoxy group) than **1a–c** whereas the variation in α_{YY} is marginal, while α_{ZZ} is almost equal.

UV–Visible spectra of **1b** and **1e** in gaseous phase have been simulated using the time dependent density functional theory (TD-DFT) Becke3-Lee–Yang–Parr hybrid functional-6-311G(d,p) method. The highest occupied molecular orbital (HOMO) and lowest unoccupied molecular orbital (LUMO) have been analyzed to describe the electronic transition properties of the systems. Theoretically predicted UV–Visible spectra of the compounds **1b** and **1e** in gaseous state is compared with the observed experimental results in $CHCl_3$ and are shown in Fig. 8. The theoretical data is in good agreement with the experimental data considering that the theoretical spectrum in gaseous phase gives an approximation. From the graphical representation of UV–Visible spectra it is clear that the absorption maxima at 340 nm is due to the electronic excitation between π–π^*orbitals. The electron density of the molecular orbitals is mainly concentrated in the aromatic region of the molecules, and the HOMO–LUMO diagram of the molecule is shown in Fig. 9a–d.

The difference between HOMO–LUMO energies (Table 4) gives an estimation of kinetic stability of the molecule and also indicates the reactivity pattern [71,72]. The HOMO–LUMO energy gap for **1b** and **1e** are found to be 3.73 eV and 3.69 eV respectively, and suggests that the compounds are fairly stable.

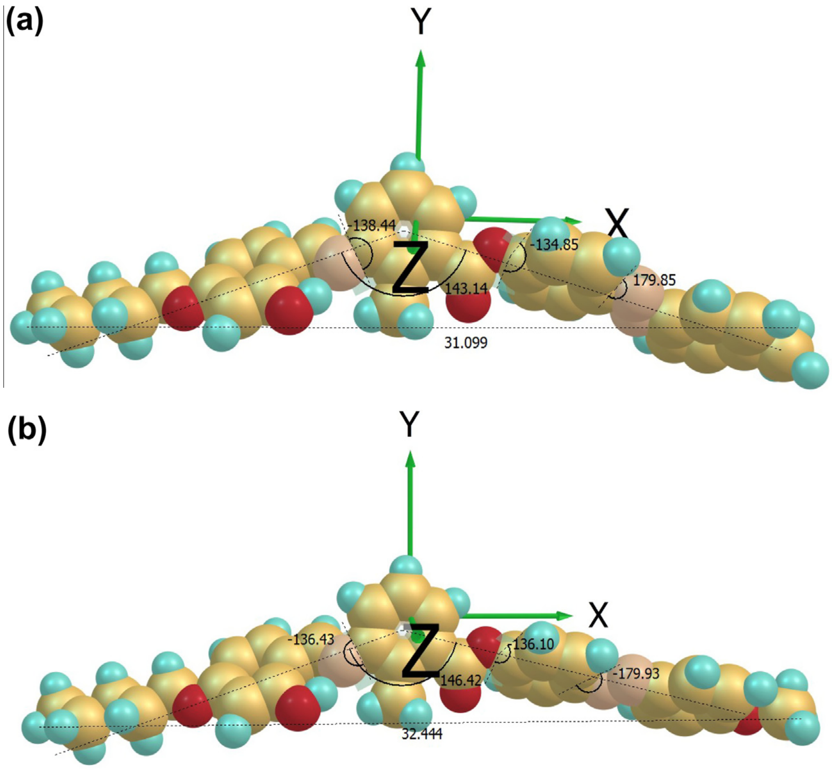

Fig. 7. DFT optimized molecular structure using B3LYP hybrid functional and the 6-311G(d,p) basis set. (a) **1b** and (b) **1e.** The bent angle is 143¯146° and the two dihedral angles (134–138°) indicate that the central phenyl ring is out-of-plane to adjacent phenyl rings. The phenyl rings with azo linkage are in the same plane.

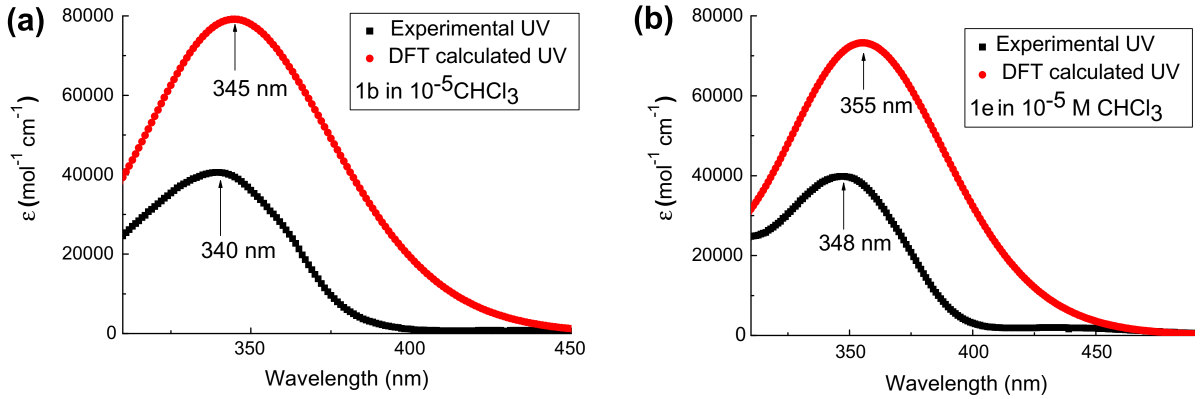

Fig. 8. Comparison of experimental UV–Visible absorption spectrum with simulated spectrum obtained from time dependent DFT 6-311G(d,p) method in gaseous phase for the compound (a) **1b** and (b) **1e**.

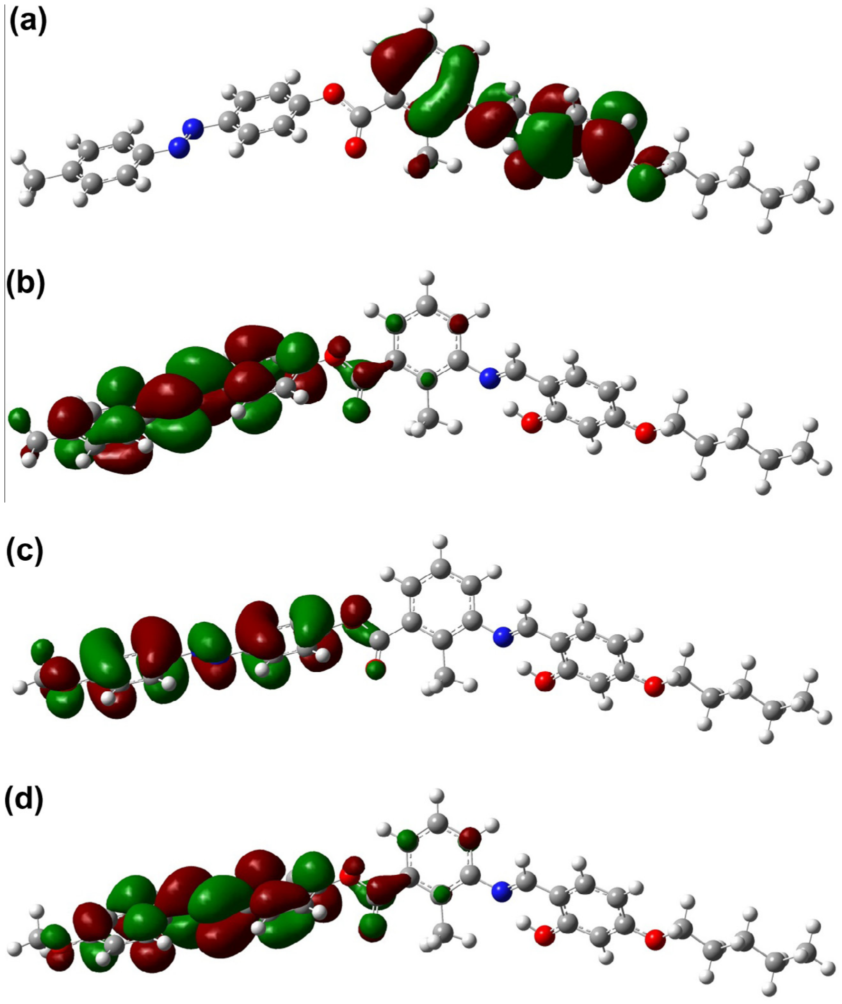

Fig. 9. HOMO and LUMO diagrams of compounds **1b** (a and b respectively)and **1e** (c and d respectively).

Table 4
Energy of HOMO, LUMO and their difference in eV.

Compounds	HOMO energy	LUMO energy	ΔE
1b	−5.77	−2.04	3.73
1e	−5.63	−1.94	3.69

5. Experimental

All the chemicals were procured from M/s Alfa Aesar or Aldrich or Tokyo Kasei Kogyo Co. Ltd. The solvents and reagents are of AR grade and were distilled and dried before use. Micro analysis of C, H and N elements were determined on Carlo-Erba 1106 elemental analyzer. IR spectra were recorded on a Shimadzu IR Prestige-21, FTIR-8400S (ν_{max} in cm^{-1}) over the 400–4000 cm^{-1} spectral range in KBr pellets. The ^{1}H NMR spectra were recorded in $CDCl_3$ solution either on JEOL AL300 FTNMR multinuclear spectrometer or Bruker AvanceIII-400 spectrometer (chemical shift δ in parts per million relative to tetramethylsilane (TMS) as internal standard). UV visible absorption spectra of the compounds in $CHCl_3$ at different concentrations were recorded either on a Shimadzu UV-1601PC spectrophotometer or Perkin–Elmer lambda35 UV–Visible spectrophotometer (λ_{max} in nm). *Trans–cis* photo-isomerization was performed in situ in an experimental setup assembled with the UV lamp. The phase transition temperatures and associated enthalpies were recorded at a heating and cooling rate 5 °C/min using differential scanning calorimetry (DSC) (Perkin–Elmer Pyris-1 system). The DSC was calibrated with indium (156.6 °C, 28.4 J/g) and tin (232.1 °C, 60.5 J/g). The liquid crystalline properties of the compounds were characterized using polarizing optical microscope (POM) (Nikon optiphot-2-pol attached with hot and cold stage HCS302, with STC200 temperature controller configured for HCS302 from INSTEC Inc. USA).

5.1. Synthesis of 4-n-butyloxy-2-hydroxybenzaldehyde (2a)

4-n-Alkoxy-2-hydroxybenzaldehydes were prepared following the earlier reported procedures [48,53]. 2,4-Dihydroxybenzaldehyde (6.9 g, 50 mmol), 1-bromobutane (6.6 g, 50 mmol), $KHCO_3$ (1 g, 50 mmol) and catalytic amount of KI were mixed in dry acetone (250 mL) and the mixture was refluxed for 48 h. It was then filtered hot to remove the insoluble solid. The warm solution was neutralized by adding dilute HCl and extracted twice with $CHCl_3$ (100 mL). The combined extract was concentrated to give a purple liquid. The product was further purified by column chromatography using silica gel (60–120 mesh) eluting with a mixture of hexane and chloroform (v/v 1:1) followed by evaporation of the solvent. The product was obtained as a pale yellow liquid. Yield: 5.8 g (60%); IR υ_{max} in cm^{-1}: 3449 (ν_{O-H}, H-bonded), 1666 ($\nu_{C=O}$, aldehyde). ^{1}H NMR ($CDCl_3$, 300 MHz): δ = 11.41 (s, 1H, —O**H**), 9.66 (s, 1H, —C**H**O), 7.41 (d, 1H, J = 8.7 Hz, Ar**H**), 6.53 (d, 1H, J = 8.7 Hz, Ar**H**), 6.62 (d, 1H, J = 2.7 Hz, Ar**H**), 4.03 (t, 2H, J = 7.8 Hz, —OC**H**$_2$—), 1.65–1.20 (m, 4H, —(C**H**$_2$)$_2$—), 0.89 (t, 3H, J = 6.6 Hz, —C**H**$_3$).

4-n-Pentyloxy and 4-n-hexyloxy-2-hydroxybenzaldehyde (***n* = 5** and **6**) were prepared following the above procedure with appropriate amount of alkyl bromides. The yield of products, spectroscopic and analytical data are presented below.

5.2. 4-n-Pentyloxy-2-hydroxybenzaldehyde (2b)

Pale yellow liquid. Yield: 6.6 g (63%). IR υ_{max} in cm^{-1}: 3449 (ν_{O-H}, H-bonded), 1666 ($\nu_{C=O}$, aldehyde). ^{1}H NMR ($CDCl_3$, 300 MHz): δ = 11.41 (s, 1H, —O**H**), 9.66 (s, 1H, —C**H**O), 7.40 (d, 1H, J = 8.7 Hz, Ar**H**), 6.51 (d, 1H, J = 8.7 Hz, Ar**H**), 6.61 (d, 1H, J = 2.7 Hz, Ar**H**), 4.03 (t, 2H, J = 7.8 Hz, —OC**H**$_2$—), 1.65–1.20 (m, 6H, —(C**H**$_2$)$_3$—), 0.89 (t, 3H, J = 6.6 Hz, —C**H**$_3$).

5.3. 4-n-Hexyloxy-2-hydroxybenzaldehyde (2c)

Pale yellow liquid. Yield: 7.4 g (67%). IR υ_{max} in cm^{-1}: 3449 (ν_{O-H}, H-bonded), 1666 ($\nu_{C=O}$, aldehyde). ^{1}H NMR ($CDCl_3$, 300 MHz): δ = 11.40 (s, 1H, —O**H**), 9.64 (s, 1H, —C**H**O), 7.40 (d, 1H, J = 8.7 Hz, Ar**H**), 6.52 (d, 1H, J = 8.7 Hz, Ar**H**), 6.62 (d, 1H, J = 2.7 Hz, Ar**H**), 4.03 (t, 2H, J = 7.8 Hz, —OC**H**$_2$—), 1.65–1.20 (m, 8H, —(C**H**$_2$)$_4$—), 0.89 (t, 3H, J = 6.6 Hz, —C**H**$_3$).

5.4. 3-Amino-2-methyl-benzoic acid

2-Methyl-3-nitrobenzoic acid (2 g, 12.12 mmol) was dissolved in ethyl acetate in a two neck round bottom flask to it 5% Pd–C (0.10 g). The reaction mixture is stirred for 15 h under balloon pressure filled with hydrogen gas. On completion of the reaction the crude product was collected by evaporating the solvent under reduced pressure. The crude product was then purified by column chromatography (silica gel 60–120 mesh, using dichloromethane and ethanol, (v/v, 99.5:0.5) as eluent to give pure white solid. mp: 181 °C. Yield: 1.5 g (90%). IR ν_{max} in cm^{-1}: 3244 (ν_{N-H}), 1724 ($\nu_{C=O}$, acid), 1284 (ν_{C-N}, aromatic amine). Elemental analysis calculated for $C_8H_9NO_2$: C, 63.56%; H, 6.00%; N, 9.27%.; Found: C, 63.13%; H, 5.87%; N, 8.99%.

5.5. 2-Methyl-3-N-(4-n-alkoxysalicylidene) amino benzoic acid (3a–3c)

The intermediate Schiff base compounds **3a–3c** were synthesized following the standard procedure reported earlier [49,50] by refluxing a mixture of ethanolic solution of 1 mmol of the 4-n-alkoxy-2-hydroxybenzaldehyde with 1 mmol of 3-amino-2-methyl-benzoic acid and few drops of glacial acetic acid as catalyst for 4 h. The precipitated product was purified by repeated recrystallization from absolute ethanol till constant clearing temperatures are achieved.

5.6. 2-Methyl-3-N-(4-n-butyloxy-2-hydroxybenzylidene) amino benzoic acid (3a)

Yellow solid. m.p.: 163 °C. Yield: 0.85 g, (78%). IR υ_{max} in cm^{-1}: 3516 (ν_{O-H}, H-bonded), 1687 ($\nu_{C=O}$, acid), 1614 ($\nu_{C=N}$, imine). ^{1}H NMR (400 MHz, $CDCl_3$): (δ_H), 13.49 (s, 1H, —**OH**), 10.06 (s, 1H, —COO**H**),8.42 (s, 1H, —C**H**=N—), 7.88 (dd, 1H, J = 1.2 Hz, J = 8.0 Hz, **ArH**), 7.32 (t, 1H, J = 8.0 Hz, **ArH**), 7.28 (d, 1H, J = 8.4 Hz, **ArH**), 7.22 (dd, 1H, J = 1.2 Hz, 8.0 Hz, **ArH**), 6.52 (dd, 1H, J = 2.4 Hz, J = 8.4 Hz, **ArH**), 6.49 (d, 1H, J = 2.4 Hz, **ArH**), 4.02 (t, 2H, J = 6.4 Hz, —**OCH$_2$**—), 2.65 (s, 3H, —**CH$_3$**—), 1.80 (q, 2H, J = 6.0 Hz, —CH$_2$**CH$_2$**CH$_2$—), 1.51 (h, 2H, J = 7.6 Hz, —CH$_2$**CH$_2$**CH$_3$—), 0.99 (t, 3H, J = 7.6 Hz, —**CH$_3$**). ^{13}C NMR (400 MHz, $CDCl_3$): (δ_C), 162.5, 134.5, 133.6, 131.7, 130.2, 128.7, 126.4, 122.7, 112.9, 107.7, 101.5, 77.3, 77.0, 76.7, 68.0, 31.0, 19.2, 15.5, 13.8. Elemental analysis calculated for $C_{19}H_{21}NO_4$: C, 69.71%; H, 6.47%; N, 4.28% Found: C, 69.23%; H, 6.22%; N, 3.96%.

5.7. 2-Methyl-3-N-(4-n-pentyloxy-2-hydroxybenzylidene) amino benzoic acid (3b)

Yellow solid, m.p.: 138 °C. Yield: 0.89 g, (78%). IR υ_{max} in cm^{-1}: 3516 (ν_{O-H}, H-bonded), 1689 ($\nu_{C=O}$, acid), 1616 ($\nu_{C=N}$, imine). ^{1}H NMR ($CDCl_3$, 400 MHz): δ = 13.52 (s, 1H, —O**H**), 10.03 (s, 1H, —COO**H**), 8.36 (s, 1H, —C**H**=N), 7.88 (d, 1H, J = 8.4 Hz, Ar**H**), 7.49 (d, 1H, J = 8.4 Hz, Ar**H**), 7.37 (t, 1H, J = 8.0 Hz, Ar**H**), 7.29 (d, 1H, J = 7.8 Hz, Ar**H**), 6.98 (d, 1H, J = 8.4 Hz, Ar**H**), 6.44 (s, 1H, Ar**H**), 4.03 (t, 2H, J = 7.8 Hz, —OC**H**$_2$—), 2.68 (s, 3H, Ar—**CH$_3$**), 1.68–1.21 (m, 6H, —(C**H**$_2$)$_3$—), 0.91 (t, 3H, J = 6.6 Hz, —C**H**$_3$). Elemental analysis calculated for $C_{20}H_{23}NO_4$: C, 70.36%; H, 6.79% Found: C, 70.06%; H, 6.42%.

5.8. 2-Methyl-3-N-(4-n-hexyloxy-2-hydroxybenzylidene) amino benzoic acid (3c)

Yellow solid, m.p.: 134 °C. Yield: 0.91 g, (77%). IR υ_{max} in cm^{-1}: 3516 (ν_{O-H}, H-bonded), 1689 ($\nu_{C=O}$, acid), 1616 (ν C=N, imine). ^{1}H NMR ($CDCl_3$, 400 MHz): δ = 13.52 (s, 1H, —O**H**), 10.03 (s, 1H, —COO**H**), 8.36 (s, 1H, —C**H**=N), 7.88 (d, 1H, J = 8.4 Hz, Ar**H**), 7.49

(d, 1H, J = 8.4 Hz, Ar**H**), 7.37 (t, 1H, J = 8.0 Hz, Ar**H**), 7.29 (d, 1H, J = 7.8 Hz, Ar**H**), 6.98 (d, 1H, J = 8.4 Hz, Ar**H**), 6.44 (s, 1H, Ar**H**), 4.03 (t, 2H, J = 7.8 Hz, —OC**H$_2$**—), 2.68 (s, 3H, Ar—**CH$_3$**), 1.68–1.21 (m, 8H, J = 6.6 Hz, —(C**H$_2$**)$_3$—), 0.91 (t, 3H, J = 6.6 Hz, —C**H**$_3$). Elemental analysis calculated for $C_{21}H_{25}NO_4$: C, 70.96%; H, 7.09%; N, 3.94% Found: C, 70.56%; H, 6.97%; N, 3.63%.

5.9. *4-Hydroxy-4′-methyl azobenzene (4a) and 4-hydroxy-4′-methoxy azobenzene (4b)*

4-Hydroxy-4′-methyl (methoxy) azobenzene was prepared following the general procedure reported earlier [73,74]. An aqueous solution of sodium nitrite (33 mmol) was added slowly with vigorous stirring to a solution of p-toluidine (30 mmol) (or p-anisidine 30 mmol) in 3 M hydrochloric acid (50 ml) at 0 °C. The resulting diazonium salt solution was then slowly added to a stirred solution of phenol (33 mmol) in 10% aqueous sodium hydroxide (40 ml) at 0 °C. The dark brown suspension was acidified and the precipitate was collected. The crude product was washed repeatedly with large quantity of water and the final yellow solid was dried under vacuum.

5.10. *4-Hydroxy-4′-methyl azobenzene (4a)*

Yellow solid, m.p.: 148 °C, Yield = 3.1 g (67%). IR υ_{max} in cm^{-1}: 3421 (υ_{O-H}), 1467($\upsilon_{N=N,}$ azo). The ^{1}H NMR data is furnished in ESI (Table S2). Elemental analysis calculated for $C_{13}H_{12}N_2O$: C, 73.56%; H, 5.70%; Found: C, 73.06%; H, 5.28%.

4-Hydroxy-4′-methoxy azobenzene (4b): Yellow solid. m.p.: 139 °C [139–141 °C, [74]], Yield = 2.8 g (66%). IR υ_{max} in cm^{-1}: 3421 (υ_{O-H}), 1467 ($\upsilon_{N=N,}$ azo). The ^{1}H NMR data is furnished in ESI (Table S2). Elemental analysis calculated for $C_{13}H_{12}N_2O_2$: C, 68.41%; H, 5.30%; Found: C, 68.02%; H, 5.23%.

5.11. *General procedure for the synthesis of compounds (1a–f)*

Appropriate quantity of substituted benzoic acid (2 mmol) (2-Methyl-3-N-(4-n-butyloxy-2-hydroxybenzylidene) amino benzoic acid, 0.65 g; 2-Methyl-3-N-(4-n-pentyloxy-2-hydroxybenzylidene) amino benzoic acid, 0.68 g; 2-Methyl-3-N-(4-n-hexyloxy-2-hydroxybenzylidene) amino benzoic acid, 0.71 g) and 4-hydroxy-4′-methoxy azobenzene (0.456 g, 2 mmol) were dissolved in dry dichloromethane (DCM) (50 mL) and catalytic amount of 4-dimethylaminopyridine (DMAP) (4 mg, 0.02 mmol) was added to the solution. A solution of N, N′-dicyclohexylcarbodiimide (DCC) (0.49 g, 2.4 mmol) was added to the reaction mixture and the mixture was stirred for 48 h under inert atmosphere at room temperature. The precipitate of N, N′-dicyclohexylurea was removed by filtration and the solvent DCM was evaporated to get crude product. The crude product was purified by column chromatography using silica gel (60–120 mesh) with hexane/ chloroform (9:1) as eluent. The yellow solid was recrystallized several times from absolute ethanol to get the pure product.

(4′-Methyl phenyl azo) phenyl-4-yl 3-[N-(4′-n-butyloxy-2-hydroxybenzylidene)amino]-2-methyl benzoate, **1a:** Yield: 0.072 g (69%). IR ν_{max} in cm^{-1}: 3170 (ν_{O-H}, H-bonded), 1743 ($\nu_{C=O}$, ester), 1610 ($\nu_{CH=N}$, imine). ^{1}H NMR (400 MHz, CDCl$_3$): (δ_H), 13.49 (s, 1H, —**OH**), 8.44 (s, 1H, —C**H**=N—), 8.00 (dd, 1H, J = 2.0 Hz, J = 6.8 Hz, **ArH**), 7.99 (dd, 2H, J = 2.8 Hz, 8.0 Hz, **ArH**), 7.84 (d, 2H, J = 8.4 Hz, **ArH**), 7.39 (dd, 2H, J = 2.0 Hz, J = 6.8 Hz, **ArH**), 7.37 (d, 1H, J = 7.6 Hz, **ArH**), 7.32 (d, 1H, J = 8.8 Hz, **ArH**), 7.31 (t, 1H, J = 9.6 Hz, **ArH**), 7.27 (d, 2H, J = 7.6 Hz, **ArH**), 6.52 (dd, 1H, J = 2.4 Hz, J = 8.4 Hz, **ArH**), 6.50 (d, 1H, J = 2.0 Hz, **ArH**), 4.02 (t, 2H, J = 6.4 Hz, —**OCH$_2$**—), 2.68 (s, 3H, —**CH$_3$**—), 2.44 (s, 3H, Ar—**CH$_3$**), 1.80 (q, 2H, J = 6.8 Hz, —CH$_2$C**H$_2$**CH$_2$—), 1.51 (h, 2H, J = 7.2 Hz, —CH$_2$C**H$_2$**CH$_3$—), 0.99 (t, 3H, J = 7.6 Hz, —**CH$_3$**). ^{13}C NMR (400 MHz, CDCl$_3$): (δ_C), 165.6, 163.8, 163.6, 162.5, 152.7, 151.0, 150.5, 149.5, 141.8, 134.5, 133.8, 130.5, 129.7, 129.3, 128.5, 126.5, 124.0, 123.0, 122.8, 122.3, 113.0, 107.5, 101.5, 77.3, 76.9, 76.7, 67.9, 31.0, 21.5, 19.2, 15.5, 13.8. Elemental Analysis calculated for $C_{32}H_{31}N_3O_3$: C, 76.02%, H, 6.18%, N, 8.31% Found: C, 76.00%, H, 6.08%, N, 8.21%.

(4′-Methyl phenyl azo) phenyl-4-yl 3-[N-(4′-n-pentyloxy-2-hydroxybenzylidene)amino]-2-methyl benzoate, **1b**: Yellow solid, Yield: 0.074 g (70%). IR ν_{max} in cm^{-1}: 3194 (ν_{O-H}, H-bonded), 1735 ($\nu_{C=O}$, ester), 1610 ($\nu_{CH=N}$, imine). Elemental Analysis calculated for $C_{33}H_{33}N_3O_3$: C, 76.28%; H, 6.40%; N, 8.09% Found: C, 76.00%; H, 6.11%; N, 7.88%.

^{1}H and ^{13}C NMR data of the compounds **1b**, **1c**, **1e** and **1f** have been furnished in ESI.

(4′-Methyl phenyl azo) phenyl-4-yl 3-[N-(4′-n-hexyloxy-2-hydroxybenzylidene)amino]-2-methyl benzoate, **1c**: Yellow solid, Yield: 0.077 g (70.12%). IR ν_{max} in cm^{-1}: 3196 (ν_{O-H}, H-bonded), 1743 ($\nu_{C=O}$, ester), 1612 ($\nu_{CH=N}$, imine). Elemental Analysis calculated for $C_{34}H_{35}N_3O_3$: C, 76.52%; H, 6.61%; N, 7.87% Found: C, 76.22%; H, 6.33%; N, 7.48%.

(4′-Methoxy phenyl azo) phenyl-4-yl 3-[N-(4′-n-butyloxy-2-hydroxybenzylidene)amino]-2-methyl benzoate, **1d**: Yellow solid, Yield: 0.075 g (70.29%). IR υ_{max} in cm^{-1}: 3192 (υ_{O-H} H-bonded); 1741 ($\upsilon_{C=O,}$ ester); 1610 ($\upsilon_{C=N,}$ imine). ^{1}H NMR (400 MHz, CDCl$_3$): (δ_H), 13.43 (s, 1H, —**OH**), 8.48 (s, 1H, —C**H**=N—), 8.03 (dd, 1H, J = 1.2 Hz, J = 8.0 Hz, **ArH**), 8.00 (dd, 2H, J = 2.0 Hz, 6.8 Hz, **ArH**), 7.96 (dd, 2H, J = 2.0 Hz, J = 6.8 Hz, **ArH**), 7.42 (t, 1H, J = 7.6 Hz, **ArH**), 7.40 (d, 1H, J = 6.4 Hz, **ArH**), 7.40 (dd, 1H, J = 2.4 Hz, J = 6.4 Hz, **ArH**), 7.33 (d, 2H, J = 8.4 Hz, **ArH**), 7.05 (dd, 2H, J = 2.0 Hz, J = 7.2 Hz, **ArH**), 6.61 (d, 1H, J = 2.0 Hz, **ArH**), 6.53 (dd, 1H, J = 2.4 Hz, J = 8.4 Hz, **ArH**), 4.05 (t, 2H, J = 6.8 Hz, —**OCH$_2$**—), 3.92 (s, 3H, —**OCH$_3$**—), 2.69 (s, 3H, Ar—**CH$_3$**), 1.82 (q, 2H, J = 7.2 Hz, —CH$_2$C**H$_2$**CH$_2$—), 1.53 (h, 2H, J = 7.2 Hz, —CH$_2$C**H$_2$**CH$_3$—), 1.01 (t, 3H, J = 7.2 Hz, —**CH$_3$**). ^{13}C NMR (400 MHz, CDCl$_3$): (δ_C), 165.7, 163.8, 162.6, 162.1, 152.3, 151.0, 150.5, 146.9, 141.8, 134.2, 133.8, 130.5, 129.7, 129.3, 128.5, 126.6, 124.8, 123.8, 122.7, 122.3, 114.2, 107.9, 101.5, 77.3, 77.0, 76.7, 68.1, 55.6, 31.0, 19.2, 15.4, 13.8. Elemental Analysis calculated for $C_{32}H_{31}N_3O_4$: C, 73.68%; H, 5.99%; N, 8.06% Found: C, 73.03%; H, 5.31%; N, 7.98%.

(4′-Methoxy phenyl azo) phenyl-4-yl 3-[N-(4′-n-pentyloxy-2-hydroxybenzylidene)amino]-2-methyl benzoate, **1e**: Yellow solid, Yield: 0.075 g (69.31%). IR υ_{max} in cm^{-1}: 3186(υ_{O-H} H-bonded); 1737 ($\upsilon_{C=O,}$ ester); 1604 ($\upsilon_{C=N,}$ imine). Elemental Analysis calculated for $C_{33}H_{33}N_3O_4$: C, 74.00%; H, 6.21%; N, 7.84% Found: C, 73.93%; H, 6.11%; N, 7.78%.

(4′-Methoxy phenyl azo) phenyl-4-yl 3-[N-(4′-n-hexyloxy-2-hydroxybenzylidene)amino]-2-methyl benzoate, **1f**: Yellow solid, Yield: 0.079 g (69.91%). IR υ_{max} in cm^{-1}: 3246(υ_{O-H} H-bonded); 1739. ($\upsilon_{C=O,}$ ester); 1610 ($\upsilon_{C=N,imine}$). Elemental Analysis calculated for $C_{34}H_{35}N_3O_4$: C, 74.29%; H, 6.42%; N, 7.64% Found: C, 73.07%; H, 6.31%; N, 7.38%.

6. Conclusions

For all future applications in the field of BLCs, it is important to draw from a wide range of compounds and different classes of substances, in order to optimize the criteria for selecting appropriate materials. Since future priorities for the specific properties cannot yet be foreseen, realization of new classes of materials remains of high importance. Achiral four ring unsymmetrical bent-core liquid crystals derived from 3-amino-2-methylbenzoic acid with imine, ester and photochromic azo linking moieties have been designed, synthesized and characterized. All the compounds exhibit wide thermal range of enantiotropic N phase. The compounds exhibit photochromic behaviour due to presence of azo group in the

Table 5
A comparison of physical parameters bend angle (Θ °), nematic-isotropic transition temperature (T_{NI} °C), nematic thermal range (ΔT_N °C), isotropic polarizability (α_{iso} Bohr^3), polarizability anisotropy ($\Delta\alpha$ Bohr^3), resultant dipole moment (μ D), and asymmetry parameter (η) of different compounds as a function of substituent polarity in four-ring bent-core system.

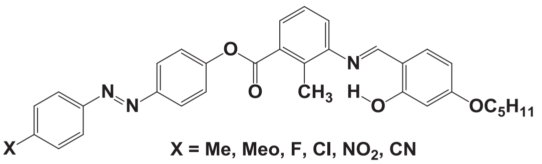

X	Me	Meo	F	Cl	NO_2	CN
Θ	143	146	146	146	147	147
T_{NI}	163.2	174.2	156.7	174.9	196.1	210.2
ΔT_N	46.6	72.0	85.3	84.1	122.4	131.3
α_{iso}	510	523	492	513	524	526
$\Delta\alpha$	604	664	605	656	671	692
μ	4.52	3.72	6.50	7.21	11.1	10.8
η	0.16	0.10	0.10	0.10	0.14	0.09

molecule. A comparison of different molecular physical parameters is presented in Table 5. The theoretical calculations predicted that the bending angle (143–147°) of all the molecules is bordering between the calamitic and bent-core molecules. The nematic-isotropic clearing temperature increases with increasing polar character of the substituent with the exception of fluoro substituent. Further the nematic thermal phase range is comparable with the five-ring oxadiazole derivatives [42,45] while it is very large when compared to seven-ring thiadiazole derivatives [70]. The isotropic polarizabilities of all the compounds are almost same because of the phenyl rings major contribution. With the exception of fluoro compound the polarizability anisotropy is reflected in the nematic thermal range. All the polar compounds possess strong dipole moment. The molecules of these compounds exhibiting nematic phase closely resemble the true hockey-stick shape rather than the compounds with a straight three-ring aromatic cores of rod-like shape possessing a meta-substituent at one end of the molecules reported earlier [75,76]. The unusual negative values of the bend-splay anisotropy, defined as the difference between the elastic constants of bend and splay $\Delta K_{31} = K_{33} - K_{11,}$ reported in **6-X (X = F, Cl)** make these compounds as attractive future materials suitable in formulating wide temperature range blue phase mixtures. Further investigations by X-ray diffraction (XRD), dielectric spectroscopy are in progress to characterize the detailed structure of this nematic phase and also to explore possible applications of these materials.

Acknowledgements

This research was supported by Department of Atomic Energy, Department of Science and Technology, Defence Research and Development Organization, Naval Research Board and Development and University Grants Commission India. The authors acknowledge Dr. P. Tandon, Lucknow University for useful discussions related to DFT studies. Central Instrumentation Laboratory (CIL) of Assam University is acknowledged for the NMR spectra and S Choudhury (CIL) was acknowledged for providing the Perkin–Elmer lambda-35 UV–Visible spectrophotometer facility.

Appendix A. Supplementary material

Supplementary data associated with this article can be found, in the online version, at http://dx.doi.org/10.1016/j.molstruc.2013.06.044.

References

[1] G. Pelzl, S. Diele, W. Weissflog, Adv. Mater. 11 (1999) 707.
[2] H. Takezoe, Y. Takanishi, Jpn. J. Appl. Phys. 45 (2006) 597.
[3] R.A. Reddy, C. Tschierske, J. Mater. Chem. 16 (2006) 907.
[4] M.B. Ros, J.L. Serrano, M.R. de la Fuente, C.L. Folcia, J. Mater. Chem. 15 (2005) 5093.
[5] T. Niori, T. Sekine, J. Watanabe, T. Furukawa, H. Takezoe, J. Mater. Chem. 6 (1996) 1231.
[6] D.R. Link, G. Natale, R.F. Shao, J.E. Maclennan, N.A. Clark, E. Korblova, D.M. Walba, Science 278 (1997) 1924.
[7] J. Harden, B. Mbanga, N. Eber, K. Fodor-Csorba, S. Sprunt, J.T. Gleeson, A. Jakli, Phys. Rev. Lett. 97 (2006) 157802.
[8] D.A. Coleman, J. Fernsler, N. Chattham, M. Nakata, Y. Takanishi, E. Korblova, D.R. Link, R.F. Shao, W.G. Jang, J.E. Maclennan, O.M. Monval, C. Boyer, W. Weissflog, G. Pelzl, L.C. Chien, D.M. Walba, J. Zasadzinski, J. Watanabe, H. Takezoe, N.A. Clark, Science 301 (2003) 1204.
[9] D.A. Coleman, C.D. Jones, M. Nakata, N.A. Clark, D.M. Walba, W. Weissflog, K. Fodor-Csorba, J. Watanabe, V. Novotna, V. Hamplova, Phys. Rev. E: Stat. Nonlinear Soft Matter Phys. 77 (2008) 021703.
[10] C.L. Folcia, J. Etxebarria, J. Ortega, M.B. Ros, Phys. Rev. E: Stat. Nonlinear Soft Matter Phys. 72 (2005) 041709.
[11] D. Pociecha, N. Vaupotic, E. Gorecka, J. Mieczkowski, K. Gomola, J. Mater. Chem. 18 (2008) 881.
[12] D.K. Yoon, R. Deb, D. Chen, E. Korblova, R. Shao, K. Ishikawa, N.V.S. Rao, D.M. Walba, I.I. Smalyukh, N.A. Clark, Proc. Natl. Acad. Sci. USA 107 (2010) 21311.
[13] R.K. Nath, R. Deb, N. Chakraborty, G. Mohiuddin, D.S.S. Rao, N.V.S. Rao, J. Mater. Chem. C 1 (2013) 663.
[14] R. Deb, R.K. Nath, M.K. Paul, N.V.S. Rao, F. Tuluri, Y. Shen, R. Shao, D. Chen, C. Zhu, I.I. Smalyukh, N.A. Clark, J. Mater. Chem. 20 (2010) 7332.
[15] C. Tschierske, D.J. Photinos, J. Mater. Chem. 20 (2010) 4263.
[16] M. Lehman, Liq. Cryst. Today 18 (2009) 31.
[17] V. Gortz, Liq. Cryst. Today 19 (2010) 37.
[18] V. Prasad, S.W. Kang, K.A. Suresh, L. Joshi, Q. Wang, S. Kumar, J. Am. Chem. Soc. 127 (2005) 17224.
[19] K. Van Le, M. Mathews, M. Chambers, J. Harden, Q. Li, H. Takezoe, A. Jakli, Phys. Rev. E: Stat. Nonlinear Soft Matter Phys. 79 (2009) 030701.
[20] H.G. Yoon, S.W. Kang, R.Y. Dong, A. Marini, K.A. Suresh, M.S. Rao, S. Kumar, Phys. Rev. E: Stat. Nonlinear Soft Matter Phys. 81 (2010) 051706.
[21] M. Hird, Y. Raoul, J.W. Goodby, H.F. Gleeson, Ferroelectrics 309 (2004) 95.
[22] G. Pelzl, A. Eremin, S. Diele, H. Kresse, W. Weissflog, J. Mater. Chem. 12 (2002) 2591.
[23] T. Niori, J. Yamamoto, H. Yokoyama, Mol. Cryst. Liq. Cryst. 409 (2004) 475.
[24] W. Weissflog, S. Sokolowski, H. Dehne, B. Das, S. Grande, M.W. Schröder, A. Eremin, S. Diele, G. Pelzl, H. Kresse, Liq. Cryst. 31 (2004) 923.
[25] C. Keith, A. Lehmann, U. Baumeister, M. Prehm, C. Tschierske, Soft Matter 6 (2010) 1704.
[26] K.M. Ferguson, M. Hird, J. Mater. Chem. 20 (2010) 3069.
[27] L.A. Madsen, T.J. Dingemans, M. Nakata, E.T. Samulski, Phys. Rev. Lett. 92 (2004) 145505.
[28] T.J. Dingemanns, L.A. Madsen, N.A. Zafiropoulos, W. Lin, E.T. Samulski, Philos. Trans. Roy. Soc. Lond. A 364 (2006) 2681.
[29] N.A. Zafiropoulos, W. Lin, E.T. Samulskii, T.J. Dingemans, S.J. Picken, Liq. Cryst. 36 (2009) 649.
[30] V. Gortz, J.W. Goodby, Chem. Commun. (2005) 3262.
[31] V. Gortz, C. Southern, N.W. Roberts, H.F. Gleeson, J.W. Goodby, Soft Matter 5 (2009) 463.
[32] S. Kang, Y. Saito, N. Watanabe, M. Tokita, Y. Takanishi, H. Takezoe, J. Watanabe, J. Phys. Chem. B 110 (2006) 5205.

[33] M.W. Schroder, S. Diele, G. Pelzl, U. Dunemann, H. Kresse, W. Weissflog, J. Mater. Chem. 13 (2003) 1877.
[34] R. Stannarius, A. Eremin, M.G. Tamba, G. Pelzl, W. Weissflog, Phys. Rev. E: Stat. Nonlinear Soft Matter Phys. 76 (2007) 061704.
[35] C.V. Yelamaggad, S. Shashikala, D.S. Shankar Rao, C.V. Lobo, S. Chandrasekhar, Angew. Chem. Int. Ed. 43 (2004) 3429.
[36] M.J. Freiser, Phys. Rev. Lett. 24 (1970) 1041.
[37] G.R. Luckhurst, Thin Solid Films 393 (2001) 40.
[38] G.R. Luckhurst, Angew. Chem. Int. Ed. 44 (2005) 2834.
[39] S.J. Picken, T.J. Dingemans, L.A. Madsen, O. Francescangeli, E.T. Samulski, Liq. Cryst. 39 (2012) 19.
[40] O. Francescangeli, V. Stanic, S.I. Torgova, A. Strigazzi, N. Scaramuzza, C. Ferrero, I.P. Dolbnya, T.M. Weiss, R. Berardi, L. Muccioli, S. Orlandi, C. Zannoni, Adv. Funct. Mater. 19 (2009) 2592.
[41] O. Francescangeli, E.T. Samulski, Soft Matter 6 (2010) 2413.
[42] O. Francescangeli, F. Vita, C. Ferrero, T.J. Dingemans, E.T. Samulski, Soft Matter 7 (2011) 895.
[43] F. Speetjens, J. Lindborg, T. Tauscher, N. LaFemina, J. Nguyen, E.T. Samulski, F. Vita, O. Francescangeli, E. Scharrer, J. Mater. Chem. 22 (2012) 22558.
[44] L. Chakraborty, N. Chakraborty, D.D. Sarkar, N.V.S. Rao, S. Aya, K.V. Le, F. Araoka, K. Ishikawa, D. Pociecha, E. Gorecka, H. Takezoe, J. Mater. Chem. C 1 (2013) 1562.
[45] G. Shanker, M. Nagaraj, A. Kocot, J.K. Vij, M. Prehm, C. Tschierske, Adv. Funct. Mater. 22 (2012) 1671.
[46] N. Avci, V. Borshch, D.D. Sarkar, R. Deb, G. Venkatesh, T. Turiv, S.V. Shiyanovskii, N.V.S. Rao, O.D. Lavrentovich, Soft Matter 9 (2013) 1066.
[47] W. Weissflog, U. Dunemann, S.F. Tandel, M.G. Tamba, H. Kresse, G. Pelzl, S. Diele, U. Baumeister, A. Eremin, S. Stern, R. Stannarius, Soft Matter 5 (2009) 1840.
[48] R.K. Nath, D.D. Sarkar, D.S.S. Rao, N.V.S. Rao, Liq. Cryst. 39 (2012) 889.
[49] D.D. Sarkar, R. Deb, N. Chakraborty, N.V.S. Rao, Liq. Cryst. 39 (2012) 1003.
[50] G. Venkatesh, K. Upadhyaya, G. Mohiuddin, N.V.S. Rao, Liq. Cryst. 40 (2013) 120.
[51] K. Upadhyaya, G. Venkatesh, G. Mohiuddin, N.V.S. Rao, Beilstein J. Org. Chem. 9 (2013) 26.
[52] G. Wang, M. Zhang, T. Zhang, J. Guan, H. Yang, RSC Adv. 2 (2012) 487–493.
[53] C.K. Lai, C.H. Chang, C.H. Tsai, J. Mater. Chem. 8 (1998) 599.
[54] K. Binnemans, Y.G. Galyametdinov, S.R. Collinsonc, D.W. Bruce, J. Mater. Chem. 8 (1998) 1551.
[55] I.C. Pintre, N. Gimeno, J.L. Serrano, M.B. Ros, I. Alonso, C.L. Folcia, J. Ortega, J. Etxebarria, J. Mater. Chem. 17 (2007) 2219.
[56] A.J.B. Loman, L.V.D. Does, A. Bantijes, I. Vulic, J. Polym. Sci. Part A: Polym. Chem. 3393 (1995) 493.
[57] C.H. Legge, G.R. Mitchell, J. Phys. D Appl. Phys. 25 (1992) 492.
[58] T.A. Krentsel, O.D. Lavrentovich, S. Kumar, Mol. Cryst. Liq. Cryst. 304 (1997) 463.
[59] Y. Lansac, M.A. Glaser, N.A. Clark, O.D. Lavrentovich, Nature 398 (1999) 54.
[60] H.M.D. Bandara, S.C. Burdette, Chem. Soc. Rev. 41 (2012) 1809.
[61] R.J.R. González, L.L. López, D.N. Rodríguez, Liq. Cryst. 38 (2011) 831.
[62] T. Garcia, L. Larios-Lopez, R.J. Rodriguez-Gonzalez, J.R. Torres-Lubian, D. Navarro-Rodriguez, Azo monomers exhibiting low layer shrinkage at the SmA-SmC transition and trans-cis light-induced isomerization, ChemPhysChem <http://dx.doi.org/10.1002/cphc.201200585>.
[63] M.J. Frisch et al., Gaussian 09, Revision B.01, Gaussian, Inc., CT, Wallingford, 2010.
[64] K. Kim, K.D. Jordan, J. Phys. Chem. 98 (1994) 10089.
[65] P.J. Stephens, F.J. Devlin, C.F. Chabalowski, M.J. Frisch, J. Phys. Chem. 98 (1994) 11623.
[66] A.R. Leach, Molecular Modelling – Principles and Applications, second ed., Pearson Education Limited, England, 2001.
[67] N.H. March, Electron Density Theory of Atoms and Molecules, Academic, London, 1992.
[68] E.S. Kryachko, E.V. Ludena, Energy Density Functional Theory of Many-Electron System, Kluwer, Dordrecht, 1990.
[69] W. Koch, M.C. Holthausen, A Chemist's Guide to Density Functional Theory, second ed., Wiley-VCH Verlag GmbH, 2001.
[70] J. Seltmann, A. Marini, B. Mennucci, S. Dey, S. Kumar, M. Lehmann, Chem. Mater. 23 (2011) 2630.
[71] K.H. Kim, Y.K. Han, J. Jung, Theor. Chem. Acc. 113 (2005) 233.
[72] J. Aihara, J. Phys. Chem. A 103 (1999) 7487.
[73] D. Stewart, C.T. Imrie, Polymer 37 (1996) 3419.
[74] C.L. Hiilemann, G.R. Van Hecke, S.R. Peak, J.B. Winther, M.A. Rudat, D.A. Kalman, M.L. White, J. Phys. Chem. 79 (1975) 1566.
[75] R. Stannarius, J. Li, W. Weissflog, Phys. Rev. Lett. 90 (2003) 022502.
[76] B. Das, S. Grande, W. Weissflog, A. Eremin, M.W. Schroder, G. Pelzl, S. Diele, H. Kresse, Liq. Cryst. 30 (2003) 529.